

Asymmetric Nafion-Coated Nanopore Electrode Arrays as Redox Cycling-Based Electrochemical Diodes

Kaiyu Fu¹, Donghoon Han², Seung-Ryong Kwon², and Paul W. Bohn^{1,2*}

¹Department of Chemistry and Biochemistry, University of Notre Dame, Notre Dame, IN 46556

²Department of Chemical and Biomolecular Engineering, University of Notre Dame, Notre Dame, IN 46556

*Author to whom correspondence should be addressed, pbohn@nd.edu

ABSTRACT

Inspired by the functioning of cellular ion channels, pore-based structures with nanoscale openings, have been fabricated and integrated into ionic circuits, *e.g.* ionic diodes and transistors, for signal processing and detection. In these systems, the nonlinear current responses arise either because asymmetric nanopore geometries break the symmetry of the ion distribution, creating unequal surface charge across the nanopore, or by coupling unidirectional electron transfer within a nanopore electrode. Here, we develop a high-performance redox cycling-based electrochemical diode by coating an asymmetric ion-exchange membrane, *i.e.* Nafion, on the top surface of a nanopore electrode array (Nafion@NEA), in which each pore in the array exhibits one or more annular electrodes. Nafion@NEAs exhibit highly sensitive and charge-selective electroanalytical measurements due to efficient redox cycling reaction, the permselectivity of Nafion, and strong confinement of redox species in the nanopore array. In addition, the top electrode of dual electrode Nafion@NEAs can serve as a voltage-controlled switch to gate ion transport within the nanopore. Thus, Nafion@NEAs can be operated as a diode by switching voltages applied to the top and bottom electrodes of the NEA, leading to a large rectification ratio, fast response times, and simplified circuitry without the need for external electrodes. By taking advantage of closely spaced and individually addressable electrodes, the redox cycling electrochemical diode has the potential for application to large-scale production and electrochemically-controlled circuit operations which go well beyond conventional electronic diodes or transistors.

KEY WORDS

Nanoscale electrochemistry, nanopore electrode arrays, redox cycling, ionic diode, Nafion, permselectivity.

Biological voltage-gated ion channels couple ion transport to electrochemical potential transfer, two important phenomena that support the function of higher organisms.¹⁻³ Modeling this behavior, ion transport at fabricated nanoscale architectures has attracted a great deal of interest, especially with the development of powerful nanofabrication techniques for complex nanostructures.⁴⁻⁸ When the size of nanochannels or nanopores approaches the thickness of the electrical double layer, unusual transport phenomena, which deviate from conventional macroscopic transport theory, are observed.⁹⁻¹² Following the seminal work by Stein *et al.* on the relation of ion transport to the surface charge of a nanochannel,¹³ a number of ion-based devices, *e.g.* ionic diodes,¹⁴⁻¹⁷ transistors,¹⁸⁻²⁰ and integrated circuits,^{21, 22} were fabricated and studied. These iontronic devices possess the ability to regulate ion flow in direction and magnitude, thus amplifying weak input signals into large output signals.²³ Typically, iontronic devices take advantage of one of two approaches to break the symmetry of the ion distribution – either by fabricating an asymmetric nanopore or by modulating the charge on the inner wall of the nanopore.²⁴⁻²⁶ In recent years, electrodes have also been embedded in the nanopore to efficiently modulate the electrostatic interaction between the ions and the nanopore at low threshold voltages.²⁷⁻²⁹ All of these approaches are non-Faradaic, involving no direct electron transfer, since the ions used are typically inert salts.

Electrochemical rectifiers represent an alternative type of iontronic device where the current rectification arises from unidirectional electron transfer.^{30, 31} The basic principle of the electrochemical rectifier relies on modification of the electrode surface with a redox moiety, like a polymer film or a tethered redox probe, allowing freely diffusing redox species to transfer electrons in one direction, while inhibiting current flow in the opposite direction.³²⁻³⁴ Electrochemical rectifiers based on self-assembled monolayer (SAM) modified electrodes usually

exhibit better unidirectional electron transfer characteristics than polymer modified electrodes, with defect-free SAMs achieving high rectification ratios by minimizing unwanted electrochemical reactions which can arise near defects.³⁵⁻³⁷

In order to further increase the rectification ratio, Mayer *et al.* proposed a generator-collector electrode system based on an interdigitated electrode array (IDEA), to regenerate the redox species through redox cycling.³⁸ However, the collection efficiency of the IDEA, as well as recently reported thin-layer electrodes,³⁹ is typically less than that achieved at nanoscale electrodes.⁴⁰⁻⁴³ Thus, we have developed and characterized a nanopore-based redox cycling system, *i.e.* nanopore electrode arrays (NEAs), where individually addressable ring and disk electrodes are vertically embedded into nanopores, thus exploiting transport characteristics not possible at the micro- or macroscale.^{44,45} Systematic investigation of surface charge and nanopore geometry effects on mass transport and electron transfer within nanopores reveal very high selectivity due to ion accumulation⁴⁶⁻⁴⁸ and membrane permselectivity.⁴⁹ In addition, we recently reported voltage-gated nanoparticle transport and controlled electrode collisions inside NEAs.⁵⁰ Thus, it is natural to exploit these phenomena to construct iontronic devices which couple ion transport to electrochemical phenomena.

In the present work, a redox cycling-based electrochemical diode was fabricated in a hierarchically organized structure by coating a Nafion membrane on top of a NEA (Nafion@NEA), thereby integrating the asymmetric ion transport characteristics of Nafion into the redox cycling system. As a widely used cation-exchange membrane, Nafion efficiently transports cations but strongly excludes anions, allowing the membrane to selectively target cations for electroanalytical sensing.⁵¹⁻⁵⁴ In addition, NEAs constitute a powerful nanopore-confined dual-electrode system to support redox cycling reactions, a common strategy to amplify

current signals by cyclically coupled reduction and oxidation reactions occurring at two closely spaced and individually addressable electrodes.^{44, 55} Thus, the intrinsically asymmetric Nafion@NEA structures facilitate rapid exchange of cationic redox species into the NEAs for highly efficient redox cycling. The Nafion@NEAs exhibit excellent selectivity, as demonstrated by comparison of $\text{Ru}(\text{NH}_3)_6^{3+}$ and $\text{Fe}(\text{CN})_6^{3-}$ redox cations and anions. The transport of redox species within the nanopore may also be controlled by the nanopore-embedded annular electrodes, leading to a facile mechanism to modulate the direction and magnitude of current flow. These characteristics may be combined under the right conditions so that the Nafion@NEAs function as low-voltage (driving potential < 0.5 V) diodes by directly connecting the top and bottom electrodes of the NEAs in a two terminal configuration. This redox-cycling based diode works at frequencies up to 1 Hz at a rectification ratio of 75 and is stable for > 100 cycles. The simplified electrical configuration and the capacity to integrate several individually addressable devices on a single chip supports the development of miniature iontronic circuits which are suitable for large-scale production and potential applications in nanofluidic logic operations.

RESULTS AND DISCUSSION

Nafion@NEA Characterization. The Nafion@NEA device shown schematically in **Figure 1(A)** has a Nafion membrane - with pores of average diameter, $d \sim 1\text{-}2$ nm, presenting negatively charged sulfonate groups⁵⁴- tightly bonded on top of the NEA structure. It allows cations to cross the membrane, while rejecting anions. In this design, the Nafion membrane controls access of charged redox species to the NEA, where redox cycling reactions subsequently occur between the top ring and bottom disk electrodes. When connecting the top and bottom

electrodes in a two-terminal configuration, the current through the NEA is significantly increased in one direction and suppressed in the opposite direction, leading to a redox cycling-based diode, **Figure 1(B)**.

Figure 1(C) depicts an electrochemical chip holding 8 NEA devices together with the Nafion membrane on top. As-spun Nafion membranes with thicknesses 100-400 nm were transferred to the top of the NEA wafer using thermal release tape, **Figures S1 and S2**, Supporting Information, SI. The resulting Nafion membrane coats the tops of the NEAs conformally without cracks or defects. In order to observe the NEA coated with the Nafion membrane by SEM, we show the edge of the Nafion film on a Nafion@NEA device in **Figure 1(D)**, clearly illustrating that the nanopores are highly ordered at large scale and that the NEAs are conformally coated by the Nafion membrane. Each NEA device consists of a 100 μm x 100 μm array with a 460 nm pitch, giving a pore density of *ca.* 5.5 pores/ μm^2 , or $\sim 5.5 \times 10^4$ electrochemically addressable nanopores total. In order to observe the multilayer structure of the Nafion@NEAs, one particular Nafion@NEA device was milled by focused ion beam (FIB). As shown in the cross sectional SEM image, **Figure 1(E)**, the conical nanopores exhibit top and bottom diameters of 200 nm and 150 nm, respectively. In the vertical direction, the NEAs present a metal-insulator-metal (MIM) stack, with the thickness of each layer being ~ 100 nm. The Nafion membrane which seals the opening of the NEA is evident at the top.

After confirming the structural integrity of the Nafion membranes, we characterized the permselectivity of the Nafion@NEA structure by comparing the electrochemical behavior of $\text{Ru}(\text{NH}_3)_6^{3+}$ and $\text{Fe}(\text{CN})_6^{3-}$ redox probes. Because it is a cation exchange membrane, the negatively charged Nafion is expected to allow only $\text{Ru}(\text{NH}_3)_6^{3+}$ to pass through the membrane

and undergo redox cycling reaction in the NEA. **Figure 2(A)** shows typical cyclic voltammograms (CVs) of 1 mM $\text{Ru}(\text{NH}_3)_6^{2+}$ and 1 mM $\text{Fe}(\text{CN})_6^{4-}$ in 1 M KCl obtained from NEA structure by fixing the top ring electrode of the NEA at a reducing potential for each redox species while the bottom electrode was swept. The anodic and cathodic limiting currents were collected from the bottom and top electrodes, respectively, at the most positive potential applied to the bottom electrode. The collection efficiency, *i.e.* the ratio of the two limiting currents, was typically *ca.* 98%. The current measured under redox cycling conditions between two working electrodes (generator-collector, GC mode) is amplified, amplification factor (AF) of 25, compared to one working electrode, non-GC mode, as shown in **Figure S3(A)**, SI. The CVs of both species change significantly in the presence of the Nafion membrane, as shown in **Figure 2(D)**. The limiting currents of $\text{Fe}(\text{CN})_6^{3-}$ ($i_{\text{Fe}(\text{CN})_6^{3-}}$) are largely suppressed while the limiting current of $\text{Ru}(\text{NH}_3)_6^{3+}$ ($i_{\text{Ru}(\text{NH}_3)_6^{3+}}$) is ~6-fold larger than the corresponding limiting current shown in **Figure 2(A)**. The measured ratio of $i_{\text{Ru}(\text{NH}_3)_6^{3+}}$ to $i_{\text{Fe}(\text{CN})_6^{3-}}$ is over 3000. Similarly, the AF of $\text{Ru}(\text{NH}_3)_6^{3+}$ in a Nafion@NEA structure under the same experimental conditions is *ca.* 200 with a collection efficiency over 99.7%, **Figure S3(B)**, SI. This further enhancement is likely due to the confined geometry of the Nafion@NEA architecture that increases the efficiency of redox cycling.

In order to confirm the effect of Nafion permselectivity on the electrochemical signals, finite element analysis was performed using COMSOL Multiphysics to calculate the concentration profiles of both redox species within the NEAs and Nafion@NEA structures. For NEAs, the simulated concentration profiles for $\text{Ru}(\text{NH}_3)_6^{3+}$, **Figure 2(B)**, and $\text{Fe}(\text{CN})_6^{3-}$, **Figure 2(C)**, are almost the same, consistent with the experimental data which show almost no selectivity between cations and anions at high concentration of supporting electrolyte (1 M KCl).

In contrast, the concentration profiles of $\text{Ru}(\text{NH}_3)_6^{3+}$, **Figure 2(E)**, and $\text{Fe}(\text{CN})_6^{3-}$, **Figure 2(F)**, are dramatically different in the Nafion@NEA structure, with $\text{Ru}(\text{NH}_3)_6^{3+}$ being strongly accumulated, while $\text{Fe}(\text{CN})_6^{3-}$ is depleted from the nanopore. The simulated CVs for both species, **Figure S4**, SI, confirm the experimental CVs. Finally, we characterized the relationship between the permselectivity of charged species by preparing Nafion membranes with different thicknesses by varying the speed of spin coating. As the Nafion becomes thicker, $i_{\text{Ru}(\text{NH}_3)_6^{3+}}$ increases, while $i_{\text{Fe}(\text{CN})_6^{3-}}$ decreases, **Figure S5**, SI.

Another factor affecting the experimental performance of Nafion@NEAs is the ionic strength. In particular, it is pertinent to ask whether the vast discrepancies in limiting currents observed in **Figure 2(D)** arise solely from the Nafion membrane or whether ionic strength-induced depletion layer effects in the NEA could play a role. Experiments described to this point were performed in 1 M KCl, so to make the comparison, experiments were repeated on an uncovered NEA structure at 1 mM KCl. As shown in **Figure S6**, SI, there is little effect on either limiting current, $i_{\text{Ru}(\text{NH}_3)_6^{3+}}$ or $i_{\text{Fe}(\text{CN})_6^{3-}}$, at lower ionic strength. Previous studies in uncovered NEAs had shown that the surface charge of nanopore dominates ion transport due to enlarged Debye screening lengths at low ionic strength,⁴⁷⁻⁴⁸ while little effect was observed at high (>1 M) ionic strengths. Thus, the vast discrepancies observed between $\text{Ru}(\text{NH}_3)_6^{3+}$ and $\text{Fe}(\text{CN})_6^{3-}$ in the Nafion@NEA system can be assigned almost exclusively to the permselective characteristics of Nafion, making it possible to preconcentrate target molecules and subsequently detect them efficiently at high ionic strength, a condition where the electrochemical detection of bio-analytes is often performed - *e.g.* [NaCl] is roughly 150 mM in physiological conditions.

Voltage-Gated Nanopore. Since Nafion serves as an efficient permselective membrane to control entry of different charged species into the NEA, the question arises as to whether it is

possible to add a further level of control on ion transport inside the NEA. Previously, we showed that the top ring electrode can gate the transport of nanoparticles into an electrochemical nanopore.⁵⁰ Following the same concept, two opposite situations were considered: the top electrode fixed at either an oxidizing (*e.g.* + 0.1 V) or a reducing potential (*e.g.* - 0.5 V) for $\text{Ru}(\text{NH}_3)_6^{3+}$ ($E^0_{\text{Ru}(\text{NH}_3)_6^{3+}} = - 0.13 \text{ V vs. Ag/AgCl}$). The bottom electrode was then swept between + 0.1 V and - 0.5 V, and the resulting CVs obtained from 1 mM $\text{Ru}(\text{NH}_3)_6^{3+}$ in 1 M KCl solution within NEAs or Nafion@NEAs are shown in **Figure 3**. For the CVs from NEAs, the limiting currents from CVs obtained with oxidizing and reducing potentials on the top electrode are almost the same, **Figure 3(A)**. However, in a Nafion@NEA structure the limiting current obtained from the $E_{TE} = -0.5 \text{ V}$ CV is roughly 6-fold larger than the limiting current obtained when $E_{TE} = +0.1 \text{ V}$, **Figure 3(B)**. Again, we tested the effect of ionic strength, **Figure S7**, SI, and found very little difference over the range 1mM – 1 M. Subsequently simulations were carried out for $E_{TE} = +0.1 \text{ V}$ and -0.5 V for both an uncovered NEA and Nafion@NEA, **Figure S8**, SI. The simulations clearly show no current asymmetry for the uncovered NEA, but consistent with the experiment in **Figure 3(B)**, a ~5-fold asymmetric current response for $E_{TE} = +0.1 \text{ V}$ and -0.5 V in the Nafion@NEA structure. These experiments and simulations clearly establish an additional current asymmetry associated with the potential applied to the top ring electrode in the nanopore, which supplements the asymmetry derived from the permselectivity of the Nafion membrane.

Next, we investigated how the potential of the top electrode, E_{TE} , affects the current response in Nafion@NEAs. In this experiment, the bottom electrode was swept in the range, $E_{BE} = + 0.1 \text{ V}$ to $- 0.5 \text{ V}$, while the top was fixed at different potentials, ranging from $- 1.0 \text{ V}$ to $+ 0.5 \text{ V}$. Each data point in **Figure 4(A)** represents the limiting current experimentally recorded from the bottom electrode, acquired either at the sweep termination at $E_{BE} = - 0.5 \text{ V}$ (yellow) or $E_{BE} =$

+ 0.1 V (blue), while the top electrode was fixed at the potential indicated on the x -axis. In both cases, minimal response is observed when the potentials E_{BE} and E_{TE} are both reducing, point (B) in **Figure 4(A)**, or both oxidizing, point (E) in the figure. In contrast, maximum limiting currents are observed when E_{BE} and E_{TE} are on opposite sides of the equilibrium potential. However, there is a clear asymmetry between the maximum limiting current for $E_{BE} > E_{TE}$ - blue curve, points (F) through (G) – and $E_{BE} < E_{TE}$ - yellow curve, points (C) through (D).

These observations can be understood as a combination of voltage gating and redox cycling effects. Independent of the bottom electrode potential, CVs obtained with positive E_{TE} values serve to discriminate against uptake of cations (gate closed condition). Thus, limiting currents obtained under these conditions are either small (point (D) in **Figure 4(A)** with E_{BE} and E_{TE} on opposite sides of E_{eq}) or zero (point (B) with E_{BE} and E_{TE} on the same side of E_{eq}). The small limiting current observed when E_{TE} is positive of E_{eq} and E_{BE} is negative of E_{eq} likely arise from redox cycling of the small number of cationic $\text{Ru}(\text{NH}_3)_6^{3+}$ species admitted to the nanopore under these gate-closed conditions. Similarly, and also independent of the bottom electrode potential, CVs obtained with negative E_{TE} values serve to facilitate the uptake of cations (gate open condition). Thus, much larger limiting currents are obtained under these conditions, points (F) through (G) in **Figure 4(A)** with E_{BE} and E_{TE} on opposite sides of E_{eq} , these arising from redox cycling of the enhanced number of cationic $\text{Ru}(\text{NH}_3)_6^{3+}$ species admitted to the nanopore under gate-open conditions. Finally, independent of the larger redox species population at negative E_{TE} values, no current is observed, point (E), when E_{BE} and E_{TE} are both positive. Thus, both electrodes contribute to the redox cycling behavior, while the top electrode alone controls the magnitude of cation uptake into the NEA nanopores. Overall, the clear current rectification represented by the behavior in **Figure 4(A)** results from both the permselectivity of the Nafion

membrane as well as the potential applied to the top (gate) electrode, E_{TE} .

Redox Cycling-Based Diode. The asymmetric current responses from Nafion@NEA structures suggest using the device as a redox cycling-based electrochemical diode. The preceding measurements all utilized four electrodes, with external reference and counter electrodes supplementing the two working electrodes. To simplify operation, we asked whether it would be possible to use only the top and bottom electrodes of the Nafion@NEA in a two-terminal configuration. The potential advantage compared to previously reported asymmetric nanopore or electrochemical rectifier approaches is that with 8 pairs of Nafion@NEAs patterned on one chip, it may be possible to assemble and connect them as a single monolithic signal processing unit to achieve an iontronic integrated circuit.

In **Figure 5(A)**, we compare three different diode configurations for NEAs (left panel) and Nafion@NEAs (right panel). Each configuration represents a different combination of two electrodes. In the left panel, the cathodic current obtained with the top and bottom nanopore electrodes connected (red) is several times larger than the comparable responses obtained when either the bottom (orange) or top (blue) electrodes are used individually. The close spacing and high collection efficiency of the two terminals in the BE-TE configuration (GC mode) are largely responsible for the large, redox-cycling based current, while the peak-shaped curves obtained for the other two configurations (non-GC mode) indicate the depletion of redox species at the nanopore electrode surface. Furthermore, there is negligible difference between CVs obtained in the three- and two-electrode configurations (**Figure S9**, SI). In the right panel of **Figure 5(A)**, the current response of the BE-TE two-electrode configuration is much larger than the current response for the other two configurations. Comparing all configurations in both panels, the BE-TE configuration in the Nafion@NEA exhibits the smallest hysteresis, which is a necessary

condition for fast diode response. Furthermore, in this configuration a large cathodic current is observed at an onset potential of -0.2 V, while a much smaller anodic current is obtained. Importantly, this unidirectional current flow occurs in a low-voltage window, comparable to electronic diode operation.

In order to boost the rectification performance of Nafion@NEAs, we investigated two further factors that contribute to rectification, *i.e.* analyte concentration and ionic strength. **Figure 5(B)** shows how analyte concentration affects rectification. The rectification ratio (RR) is defined as the ratio of the current at -0.5 V ($i_{-0.5\text{ v}}$) to the current at $+0.5$ V ($i_{+0.5\text{ v}}$), *i.e.* $RR = i_{-0.5\text{ v}} / i_{+0.5\text{ v}}$. Both $i_{-0.5\text{ v}}$ (blue) and $i_{+0.5\text{ v}}$ (orange) increase going to higher analyte concentrations. However, the faster increase of the cathodic current with analyte concentration above $100\text{ }\mu\text{M}$ means that RR increases rapidly as well, reaching a maximum value of 76 for $10\text{ mM Ru(NH}_3)_6^{3+}$ in 1 M KCl . To understand the effect of the magnitude of the analyte charge on the rectifying current, we investigated different ratios of $\text{Ru(NH}_3)_6^{3+}$ to $\text{Ru(NH}_3)_6^{2+}$, ranging from 1:0, 1:1 to 0:1 (**Figure S10**, SI), as well as a completely different redox pair, *e.g.* $\text{Fc}^{0/+}$ (**Figure S11**, SI).

We also explored the ionic strength dependence of the rectifying current of Nafion@NEAs. **Figure 5(C)** shows $i_{-0.5\text{ v}}$, $i_{+0.5\text{ v}}$, and RR obtained from $1\text{ mM Ru(NH}_3)_6^{3+}$ in KCl solution of varying concentrations, ranging from 0.1 mM to 1 M . Previously, we demonstrated that $\text{Ru(NH}_3)_6^{3+}$ accumulates strongly inside NEAs due to overlapping surface double layers at low ionic strength, typically μM and below. Below 100 mM , both anodic and cathodic currents from $1\text{ mM Ru(NH}_3)_6^{3+}$ show modest decreases with increasing electrolyte concentration becomes higher. However, the cathodic current increases significantly at 1 M KCl , leading to an increase of RR to a maximum value of 34 for $1\text{ mM Ru(NH}_3)_6^{3+}$ in 1 M KCl .

Diode Operation. Having demonstrated current rectification in Nafion@NEAs and identified the experimental conditions under which it is maximized, the natural next step is to explore operating the device as a redox cycling-based electrochemical diode. **Figure 6** shows the current response from multiple potential steps applied across the bottom and top electrodes. The current response was obtained for 1 mM $\text{Ru}(\text{NH}_3)_6^{3+}$ in 1 M KCl solution as a function of time by applying potential steps of different magnitudes, ranging from ± 0.1 V to ± 0.5 V, for 5 cycles at 0.1 Hz, **Figure 6(A)**. Small anodic current and cathodic currents are observed when the applied potential pair is ± 0.1 V, **Figure 6(A)** inset, since the formal potential of $\text{Ru}(\text{NH}_3)_6^{3+}$ is -0.13 V. For larger potential excursions, larger cathodic currents are observed, beginning at ± 0.2 V. The cathodic current then increases monotonically at larger potential excursions, as does the RR, which maximizes at $\text{RR} = 67$ at ± 0.4 V.

Another important parameter to characterize diode behavior is the switching time between forward and reverse bias conditions, which ultimately limits the frequency bandwidth. Most iontronic diodes exhibit relatively slow responses ($\tau > 5$ s). The Nafion@NEA diode studied here displayed faster current decays, permitting bandwidths in excess of 1 Hz, **Figure 6(B)**. The temporal response of ion-based electrochemical diodes is ultimately limited by ion transport, which dictates the length of time needed to reach an equilibrium ion distribution. In the Nafion@NEAs, the diffusion time (τ_d) between electrodes spaced by 100 nm gap is ~ 7.5 μs based on $D_{\text{ox}} \sim 6.7 \times 10^{-6} \text{ cm}^2 \text{ s}^{-1}$ for $\text{Ru}(\text{NH}_3)_6^{3+}$. Thus, rapid diffusion between two closely-spaced electrodes allows the redox species to quickly return to an equilibrium distribution inside the NEA, leading to a more rapid response.^{53, 56} In **Figure 6(B)**, we indeed observed fast current decay, reaching steady state in $\tau < 0.1$ s in both directions. Finally, the stability of Nafion@NEA was tested. As shown in **Figure 6(C)**, the Nafion@NEAs are very stable –

showing no measurable decay in performance over 100 10-s cycles, leading to an operation time of >1000 s.

CONCLUSIONS

In summary, we developed a hierarchically-organized redox cycling-based electrochemical diode by coating defect-free Nafion membranes of thickness 100-400 nm on the top of a nanopore electrode arrays (Nafion@NEA). Nafion membranes function as efficient molecular sieves, allowing only cations to be transported into the interior volume of the NEA while repelling anions. In addition, the top ring electrode of dual electrode NEAs was shown to be competent to control ion transport for subsequent redox cycling reaction inside Nafion@NEA structure, *i.e.* switching between “gate open” and “gate close”. We further simplified the electrical connection by using the top electrode and bottom electrode of NEAs in a two-terminal configuration, in which the structure exhibited strong rectification and functioned as an electrochemical diode. Together these results establish a high-performance redox cycling-based electrochemical diode with a low operation voltage, fast response and good stability. One would expect that other electrochemical diodes, *e.g.* using the transport of negatively charged species, could be produced with the same approach. To illustrate this principle, we are developing electrochemical diodes that incorporate stimulus-responsive materials, thus achieving ion rectification modulated by external stimuli. We believe that the design of the iontronic diode described here will serve to guide the fabrication of miniaturized active devices for potential applications of next-generation iontronics.

METHODS

Chemicals and Materials. Nafion 117 solution (~5% in a mixture of lower aliphatic alcohols and water), hexaammineruthenium(III) chloride ($\text{Ru}(\text{NH}_3)_6\text{Cl}_3$), hexaammineruthenium(II) chloride ($\text{Ru}(\text{NH}_3)_6\text{Cl}_2$), potassium ferricyanide(III) ($\text{K}_3\text{Fe}(\text{CN})_6$), ferrocene (Fc), ferrocenium hexafluorophosphate (FcPF_6), and potassium chloride (KCl) were obtained from Sigma-Aldrich, U.S. and used as received without purification. Deionized (DI) water ($\rho \sim 18 \text{ M}\Omega \text{ cm}$) purified using a Millipore Milli-Q system was used to prepare all aqueous solutions for electrochemical measurements. All analyte solution were prepared by dissolving calculated amount of redox species into aqueous KCl . Single-side thermal release tape (REVALPHA) was received from Nitto Denko Corporation. PDMS reservoirs were prepared by the procedures listed in the data sheet of Dow Corning Sylgard 184 silicone elastomer kit.

Device Fabrication and Characterization. The Nanopore electrode arrays (NEAs) were fabricated by sequential photolithography, metal deposition, nanosphere lithography and multistep reactive ion etching processes, following previously published procedures from this laboratory.⁴⁴ ⁵⁵ The Nafion membrane was formed on pre-cleaned silicon (Si) wafer by spin-coating 5% Nafion 117 solution at speeds ranging from 500 to 4000 rpm for 60 s. The thickness of Nafion membranes were measured by a Filmetric F20 as illustrated in **Figure S1**, SI. As-spun Nafion membranes together with Si (Nafion@Si) were heated at 60 °C for 30 min to evaporate the remaining solvent. Then, thermal release tape (TRT) was used to cover the top of the Nafion@Si substrate, *i.e.* TRT@Nafion@Si. Nafion together with TRT (TRT@Nafion) was easily peeled from Si by immersing the TRT@Nafion@Si substrate in DI water. Afterwards, the TRT@Nafion was rinsed with DI water, blown by dry N_2 gas and subsequently placed on a low power O_2 plasma-treated NEA device. Finally, the TRT@Nafion@NEA was heated at 120 °C for 30 s to release the TRT from the surface of Nafion@NEAs and then was kept at this temperature for 1 h to tightly bond

the Nafion membrane to the NEA device (details of Nafion transfer are shown in **Figure S2**, SI). SEM images of Nafion@NEA were acquired by a FEI-Helios Dual Beam FIB at an accelerating voltage of 5 kV.

Electrochemical Measurements. Cyclic voltammetry (CV) was performed on a CHI bipotentiostat (CH Instruments, Model 842C), where the first and second working electrodes were connected to the bottom disk and top ring electrode of the NEA device, respectively. Platinum (Pt) wire and Ag/AgCl electrodes were used as counter and reference electrodes, respectively. During electrochemical measurements, the Pt wire and Ag/AgCl electrodes were immersed in a 100 μ L solution inside a PDMS reservoir, covering the center region (6 mm in diameter) of the Nafion@NEA device. In all CV measurements, the top electrode was held at a constant potential, while the potential of the bottom electrode in the array was scanned at 100 mV s^{-1} , unless otherwise specified. For the electrochemical measurements and diode operation in the two electrode configuration, the bottom and top electrodes were connected to the working and reference/counter electrodes, respectively.

ASSOCIATED CONTENT

Supporting Information

Supporting Information is available free of charge on the ACS Publication website at <http://pubs.acs.org>, including 1. Characterization and transfer of Nafion; 2. Nafion@NEAs electrochemical characterization of Nafion@NEAs; 3. Asymmetric current from Nafion@NEAs; 4. Nafion@NEAs as diode. 5. Details of the finite element simulations.

AUTHOR INFORMATION

Corresponding Author

* P.W. Bohn. E-mail: pbohn@nd.edu

ORCID

Kaiyu Fu: 0000-0002-7899-0388

Donghoon Han: 0000-0003-1870-3006

Seung-Ryong Kwon: 0000-0002-0890-523X

Paul W. Bohn: 0000-0001-9052-0349

ACKNOWLEDGMENT

This work was supported by the Department of Energy (Grant DE FG02 ER15851). K.F. was supported by an ACS Division of Analytical Chemistry graduate student fellowship, which was sponsored by Eastman Chemical Company. We gratefully acknowledge Notre Dame Nanofabrication Facility and Integrated Imaging Facility for providing fabrication and structural characterization of the devices studied here. We thank Neil Dodson for his support of multiplexer design.

REFERENCES

- (1) Di Ventra, M.; Taniguchi, M., Decoding DNA, RNA and Peptides with Quantum Tunnelling. *Nat. Nanotechnol.* **2016**, *11*, 117-126.

- (2) Fu, K.; Bohn, P. W., Nanopore Electrochemistry: A Nexus for Molecular Control of Electron Transfer Reactions. *ACS Cent. Sci.* **2018**, *4*, 20-29.
- (3) Zhang, Z.; Wen, L. P.; Jiang, L., Bioinspired Smart Asymmetric Nanochannel Membranes. *Chem. Soc. Rev.* **2018**, *47*, 322-356.
- (4) Daiguji, H.; Yang, P. D.; Majumdar, A., Ion Transport in Nanofluidic Channels. *Nano Lett.* **2004**, *4*, 137-142.
- (5) Krapf, D.; Quinn, B. M.; Wu, M. Y.; Zandbergen, H. W.; Dekker, C.; Lemay, S. G., Experimental Observation of Nonlinear Ionic Transport at the Nanometer Scale. *Nano Lett.* **2006**, *6*, 2531-2535.
- (6) Sparreboom, W.; van den Berg, A.; Eijkel, J. C., Principles and Applications of Nanofluidic Transport. *Nat. Nanotechnol.* **2009**, *4*, 713-720.
- (7) Daiguji, H., Ion Transport in Nanofluidic Channels. *Chem. Soc. Rev.* **2010**, *39*, 901-911.
- (8) Sparreboom, W.; van den Berg, A.; Eijkel, J. C. T., Transport in Nanofluidic Systems: A Review of Theory and Applications. *New J. Phys.* **2010**, *12*, 015004.
- (9) van der Heyden, F. H.; Bonthuis, D. J.; Stein, D.; Meyer, C.; Dekker, C., Power Generation by Pressure-Driven Transport of Ions in Nanofluidic Channels. *Nano Lett.* **2007**, *7*, 1022-1025.
- (10) Bocquet, L.; Charlaix, E., Nanofluidics, from Bulk to Interfaces. *Chem. Soc. Rev.* **2010**, *39*, 1073-1095.
- (11) Lan, W. J.; Holden, D. A.; Zhang, B.; White, H. S., Nanoparticle Transport in Conical-Shaped Nanopores. *Anal. Chem.* **2011**, *83*, 3840-3847.

- (12) Branagan, S. P.; Contento, N. M.; Bohn, P. W., Enhanced Mass Transport of Electroactive Species to Annular Nanoband Electrodes Embedded in Nanocapillary Array Membranes. *J. Am. Chem. Soc.* **2012**, *134*, 8617-8624.
- (13) Stein, D.; Kruithof, M.; Dekker, C., Surface-Charge-Governed Ion Transport in Nanofluidic Channels. *Phys. Rev. Lett.* **2004**, *93*, 035901.
- (14) Cheng, L.-J.; Guo, L. J., Nanofluidic Diodes. *Chem. Soc. Rev.* **2010**, *39*, 923-938.
- (15) Vlassiouk, I.; Kozel, T. R.; Siwy, Z. S., Biosensing with Nanofluidic Diodes. *J. Am. Chem. Soc.* **2009**, *131*, 8211-8220.
- (16) Vlassiouk, I.; Siwy, Z. S., Nanofluidic Diode. *Nano Lett.* **2007**, *7*, 552-556.
- (17) Karnik, R.; Duan, C. H.; Castelino, K.; Daiguji, H.; Majumdar, A., Rectification of Ionic Current in A Nanofluidic Diode. *Nano Lett.* **2007**, *7*, 547-551.
- (18) Tybrandt, K.; Larsson, K. C.; Richter-Dahlfors, A.; Berggren, M., Ion Bipolar Junction Transistors. *Proc. Natl. Acad. Sci. U.S.A.* **2010**, *107*, 9929-9932.
- (19) Paik, K. H.; Liu, Y.; Tabard-Cossa, V.; Waugh, M. J.; Huber, D. E.; Provine, J.; Howe, R. T.; Dutton, R. W.; Davis, R. W., Control of DNA Capture by Nanofluidic Transistors. *ACS Nano* **2012**, *6*, 6767-6775.
- (20) Zhang, Y.; Clausmeyer, J.; Babakinejad, B.; Cordoba, A. L.; Ali, T.; Shevchuk, A.; Takahashi, Y.; Novak, P.; Edwards, C.; Lab, M.; Gopal, S.; Chiappini, C.; Anand, U.; Magnani, L.; Coombes, R. C.; Gorelik, J.; Matsue, T.; Schuhmann, W.; Klenerman, D.; Sviderskaya, E. V. *et al.*, Spearhead Nanometric Field-Effect Transistor Sensors for Single-Cell Analysis. *ACS Nano* **2016**, *10*, 3214-3221.
- (21) Han, J.-H.; Kim, K. B.; Kim, H. C.; Chung, T. D., Ionic Circuits Based on Polyelectrolyte Diodes on A Microchip. *Angew. Chem. Int. Ed. Engl.* **2009**, *48*, 3830-3833.

- (22) Tybrandt, K.; Forchheimer, R.; Berggren, M., Logic Gates Based on Ion Transistors. *Nat. Commun.* **2012**, *3*, 871.
- (23) Chun, H. G.; Chung, T. D., Iontronics. *Annu. Rev. Anal. Chem.* **2015**, *8*, 441-462.
- (24) Prakash, S.; Conlisk, A. T., Field Effect Nanofluidics. *Lab Chip* **2016**, *16*, 3855-3865.
- (25) Guo, W.; Tian, Y.; Jiang, L., Asymmetric Ion Transport through Ion-Channel-Mimetic Solid-State Nanopores. *Acc. Chem. Res.* **2013**, *46*, 2834-2846.
- (26) Lan, W. J.; Edwards, M. A.; Luo, L.; Perera, R. T.; Wu, X. J.; Martin, C. R.; White, H. S., Voltage-Rectified Current and Fluid Flow in Conical Nanopores. *Acc. Chem. Res.* **2016**, *49*, 2605-2613.
- (27) Nam, S. W.; Rooks, M. J.; Kim, K. B.; Rosnagel, S. M., Ionic Field Effect Transistors with Sub-10 nm Multiple Nanopores. *Nano Lett.* **2009**, *9*, 2044-2048.
- (28) Liu, Y.; Yobas, L., Slowing DNA Translocation in A Nanofluidic Field-Effect Transistor. *ACS Nano* **2016**, *10*, 3985-3994.
- (29) Ren, R.; Zhang, Y.; Nadappuram, B. P.; Akpınar, B.; Klenerman, D.; Ivanov, A. P.; Edel, J. B.; Korchev, Y., Nanopore Extended Field-Effect Transistor for Selective Single-Molecule Biosensing. *Nat. Commun.* **2017**, *8*, 586.
- (30) Abruna, H. D.; Denisevich, P.; Umana, M.; Meyer, T. J.; Murray, R. W., Rectifying Interfaces Using Two-Layer Films of Electrochemically Polymerized Vinylpyridine and Vinylbipyridine Complexes of Ruthenium and Iron on Electrodes. *J. Am. Chem. Soc.* **1981**, *103*, 1-5.
- (31) Alleman, K. S.; Weber, K.; Creager, S. E., Electrochemical Rectification at A Monolayer-Modified Electrode. *J. Phys. Chem.* **1996**, *100*, 17050-17058.

- (32) Oh, S. K.; Baker, L. A.; Crooks, R. M., Electrochemical Rectification Using Mixed Monolayers of Redox-Active Ferrocenyl Dendrimers and n-Alkanethiols. *Langmuir* **2002**, *18*, 6981-6987.
- (33) Guo, X.; Myers, M.; Xiao, S.; Lefenfeld, M.; Steiner, R.; Tulevski, G. S.; Tang, J.; Baumert, J.; Leibfarth, F.; Yardley, J. T.; Steigerwald, M. L.; Kim, P.; Nuckolls, C., Chemoresponsive Monolayer Transistors. *Proc. Natl. Acad. Sci. U.S.A.* **2006**, *103*, 11452-11456.
- (34) Asadi, K.; Wu, Y.; Gholamrezaie, F.; Rudolf, P.; Blom, P. W. M., Single-Layer Pentacene Field-Effect Transistors Using Electrodes Modified with Self-Assembled Monolayers. *Adv. Mater.* **2009**, *21*, 4109-4114.
- (35) Mathijssen, S. G.; Smits, E. C.; van Hal, P. A.; Wondergem, H. J.; Ponomarenko, S. A.; Moser, A.; Resel, R.; Bobbert, P. A.; Kemerink, M.; Janssen, R. A.; de Leeuw, D. M., Monolayer Coverage and Channel Length Set the Mobility in Self-Assembled Monolayer Field-Effect Transistors. *Nat. Nanotechnol.* **2009**, *4*, 674-680.
- (36) Liu, Y.; Offenhausser, A.; Mayer, D., An Electrochemically Transduced XOR Logic Gate at the Molecular Level. *Angew. Chem. Int. Ed. Engl.* **2010**, *49*, 2595-2598.
- (37) Nijhuis, C. A.; Reus, W. F.; Barber, J. R.; Dickey, M. D.; Whitesides, G. M., Charge Transport and Rectification in Arrays of SAM-Based Tunneling Junctions. *Nano Lett.* **2010**, *10*, 3611-3619.
- (38) Liu, Y.; Wolfrum, B.; Huske, M.; Offenhausser, A.; Wang, E.; Mayer, D., Transistor Functions Based on Electrochemical Rectification. *Angew. Chem. Int. Ed. Engl.* **2013**, *52*, 4029-4032.
- (39) Park, S.; Park, J. H.; Hwang, S.; Kwak, J., Programmable Electrochemical Rectifier Based on a Thin-Layer Cell. *ACS Appl. Mater. Interfaces* **2017**, *9*, 20955-20962.

- (40) Byers, J. C.; Paulose Nadappuram, B.; Perry, D.; McKelvey, K.; Colburn, A. W.; Unwin, P. R., Single Molecule Electrochemical Detection in Aqueous Solutions and Ionic Liquids. *Anal. Chem.* **2015**, *87*, 10450-10456.
- (41) Fan, F.-R. F.; Kwak, J.; Bard, A. J., Single Molecule Electrochemistry. *J. Am. Chem. Soc.* **1996**, *118*, 9669-9675.
- (42) Kang, S.; Nieuwenhuis, A. F.; Mathwig, K.; Mampallil, D.; Lemay, S. G., Electrochemical Single-Molecule Detection in Aqueous Solution Using Self-Aligned Nanogap Transducers. *ACS Nano* **2013**, *7*, 10931-10937.
- (43) Sun, P.; Mirkin, M. V., Electrochemistry of Individual Molecules in Zeptoliter Volumes. *J. Am. Chem. Soc.* **2008**, *130*, 8241-8250.
- (44) Fu, K.; Han, D.; Ma, C.; Bohn, P. W., Electrochemistry at Single Molecule Occupancy in Nanopore-Confined Recessed Ring-Disk Electrode Arrays. *Faraday Discuss.* **2016**, *193*, 51-64.
- (45) Han, D.; Zaino, L. P.; Fu, K.; Bohn, P. W., Redox Cycling in Nanopore-Confined Recessed Dual-Ring Electrode Arrays. *J. Phys. Chem. C* **2016**, *120*, 20634-20641.
- (46) Fu, K. Y.; Han, D.; Ma, C. X.; Bohn, P. W., Ion Selective Redox Cycling in Zero-Dimensional Nanopore Electrode Arrays at Low Ionic Strength. *Nanoscale* **2017**, *9*, 5164-5171.
- (47) Ma, C.; Contento, N. M.; Bohn, P. W., Redox Cycling on Recessed Ring-Disk Nanoelectrode Arrays in the Absence of Supporting Electrolyte. *J. Am. Chem. Soc.* **2014**, *136*, 7225-7228.

- (48) Ma, C. X.; Xu, W.; Wichert, W. R. A.; Bohn, P. W., Ion Accumulation and Migration Effects on Redox Cycling in Nanopore Electrode Arrays at Low Ionic Strength. *ACS Nano* **2016**, *10*, 3658-3664.
- (49) Fu, K.; Bohn, P. W., Nanochannel Arrays for Molecular Sieving and Electrochemical Analysis by Nanosphere Lithography Templated Graphoepitaxy of Block Copolymers. *ACS Appl. Mater. Interfaces* **2017**, *9*, 24908-24916.
- (50) Fu, K.; Han, D.; Crouch, G. M.; Kwon, S.-R.; Bohn, P. W., Voltage-Gated Nanoparticle Transport and Collisions in Attoliter-Volume Nanopore Electrode Arrays. *Small* **2018**, *9*, 1703248.
- (51) Szentirmay, M. N.; Martin, C. R., Ion-Exchange Selectivity of Nafion Films on Electrode Surfaces. *Anal. Chem.* **1984**, *56*, 1898-1902.
- (52) Ugo, P.; Moretto, L. M.; Bellomi, S.; Menon, V. P.; Martin, C. R., Ion-Exchange Voltammetry at Polymer Film-Coated Nanoelectrode Ensembles. *Anal. Chem.* **1996**, *68*, 4160-4165.
- (53) He, D.; Madrid, E.; Aaronson, B. D. B.; Fan, L.; Doughty, J.; Mathwig, K.; Bond, A. M.; McKeown, N. B.; Marken, F., A Cationic Diode Based on Asymmetric Nafion Film Deposits. *ACS Appl. Mater. Interfaces* **2017**, *9*, 11272-11278.
- (54) Mauritz, K. A.; Moore, R. B., State of Understanding of Nafion. *Chem. Rev.* **2004**, *104*, 4535-4586.
- (55) Ma, C.; Contento, N. M.; Gibson, L. R., 2nd; Bohn, P. W., Redox Cycling in Nanoscale-Recessed Ring-Disk Electrode Arrays for Enhanced Electrochemical Sensitivity. *ACS Nano* **2013**, *7*, 5483-5490.

(56) Cayre, O. J.; Chang, S. T.; Velev, O. D., Polyelectrolyte Diode: Nonlinear Current

Response of A Junction Between Aqueous Ionic Gels. *J. Am. Chem. Soc.* **2007**, *129*, 10801-10806.

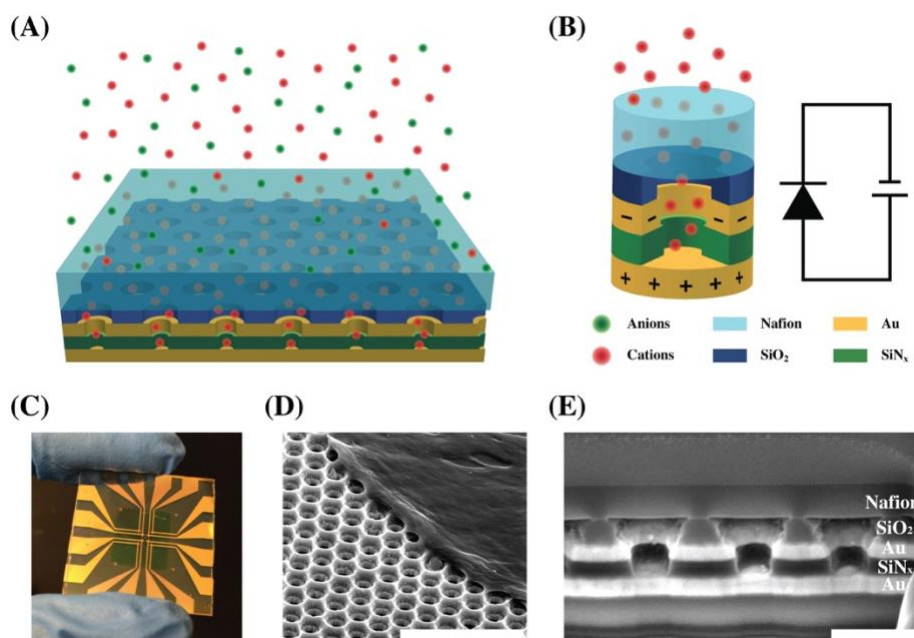


Figure 1. Schemes and SEM images of asymmetric Nafion-coated nanopore electrode arrays, Nafion@NEA. (A) Schematic illustration of Nafion@NEA, where Nafion (light blue) acts as a cation exchange membrane to allow cations (red spheres) to pass through, while rejecting anions (green spheres), for subsequent redox cycling inside the NEA. (B) The Nafion@NEA acts as a redox cycling-based diode when using the top and bottom electrodes are operated in a two terminal configuration. (C) Photo of an electrochemical diode wafer consisting of 8 NEA devices and covered by a Nafion membrane (green). (D) Tilted SEM image near the edge of the Nafion film, indicating that the Nafion conformally coats the NEA. Scale bar is 2 μm . (E) Cross-sectional SEM image showing the stacked metal (disk)-insulator-metal (ring) (MIM) structure in the vertical direction, as well the well-sealed Nafion at the top. Scale bar is 400 nm.

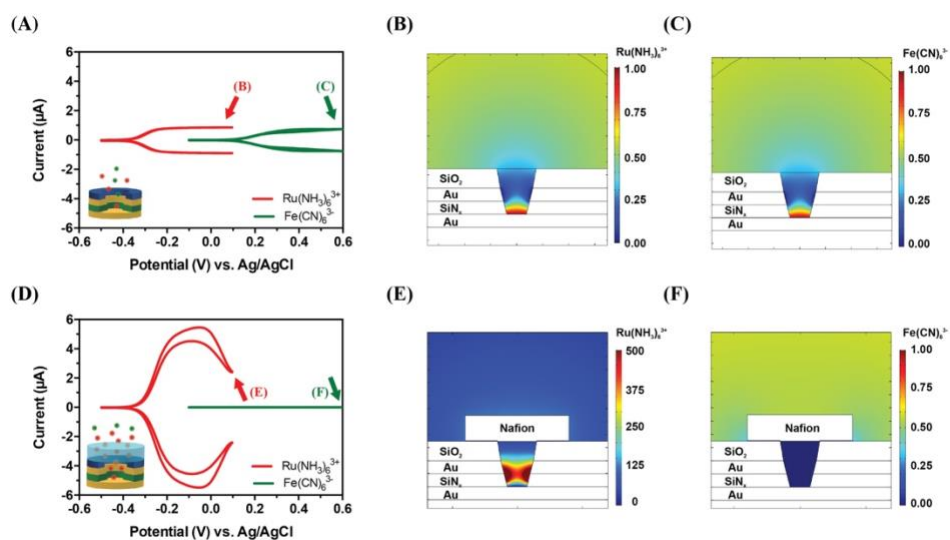


Figure 2. Electrochemical behavior of Nafion@NEAs. (A) and (D) are cyclic voltammograms (CVs) of 1 mM Ru(NH₃)₆³⁺ (red) or 1 mM Fe(CN)₆³⁻ (green) in 1 M KCl obtained at an open (no Nafion) NEA (A) and a Nafion@NEA (D). All CVs were obtained by sweeping the bottom electrode, while fixing the top electrode at a reducing potential. (B) and (C) present concentration profiles obtained from finite element simulations of Ru(NH₃)₆³⁺, (B), and Fe(CN)₆³⁻, (C), within an uncovered NEA. (E) and (F) show similar simulated concentration profiles of Ru(NH₃)₆³⁺, (E), and Fe(CN)₆³⁻, (F), obtained for a Nafion@NEA structure. The simulations are carried out at the experimental conditions marked by arrows in (A) and (D).

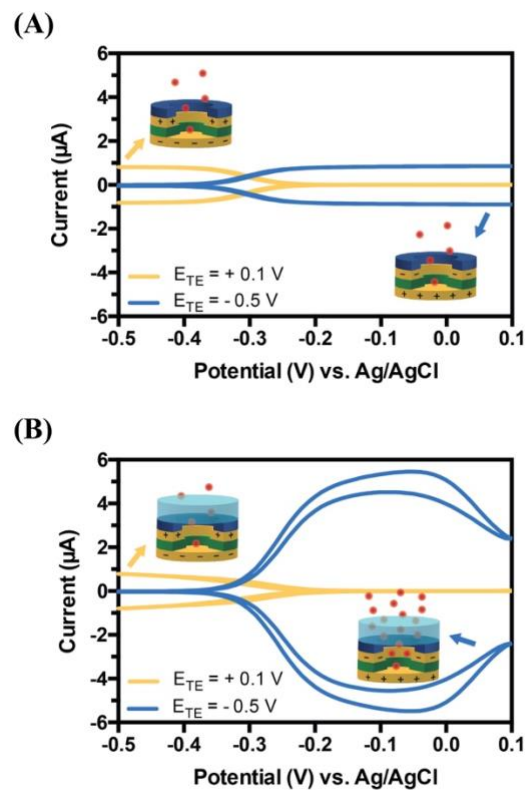


Figure 3. Asymmetric current response from Nafion@NEAs. CVs of 1 mM $\text{Ru}(\text{NH}_3)_6^{3+}$ in 1 M KCl from an uncovered NEA, (A), and Nafion@NEA, (B). For both panels, the currents are shown for $E_{TE} = +0.1$ V (yellow) and $E_{TE} = -0.5$ V (blue). The insets schematically illustrate the potential polarity marked by the arrows in (A) and (B).

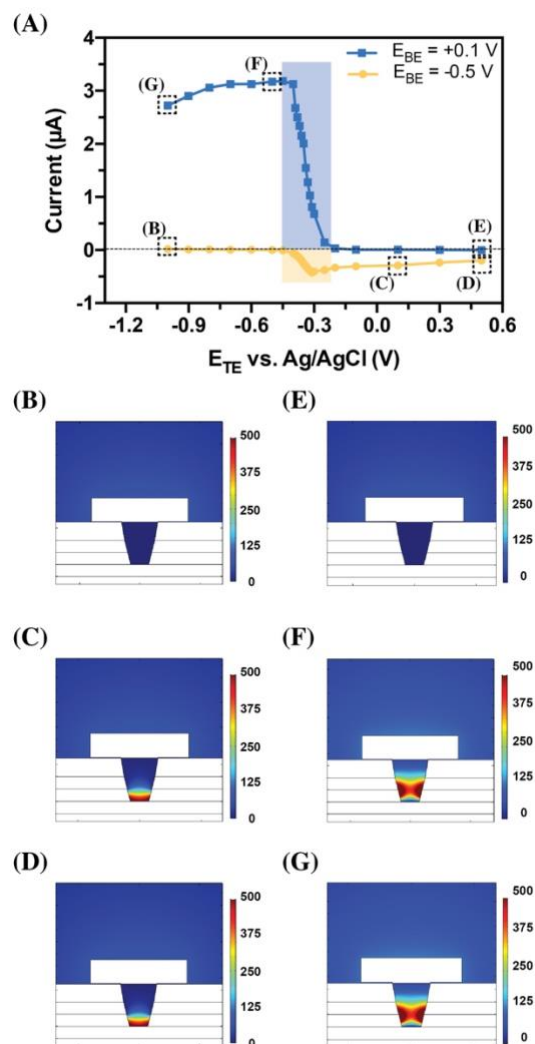


Figure 4. Voltage-gated ion transport in Nafion@NEAs. (A) Limiting current magnitudes obtained from CVs of 1 mM $\text{Ru}(\text{NH}_3)_6^{3+}$ ($E^0 = -0.30$ V vs. Ag/AgCl) in 1 M KCl at the bottom electrode. Limiting currents were obtained at $E_{BE} = +0.1$ V (blue, positive sweeps) or -0.5 V (yellow, negative sweeps), while E_{TE} was fixed at different values, ranging from -1.0 V to $+0.5$ V. The blue and yellow rectangles denote the voltage threshold range for ion gating. (B) to (G) are simulated concentration profiles calculated for the corresponding voltage conditions, (B) through (G), in panel (A) representing closed, partially open, and fully open conditions.

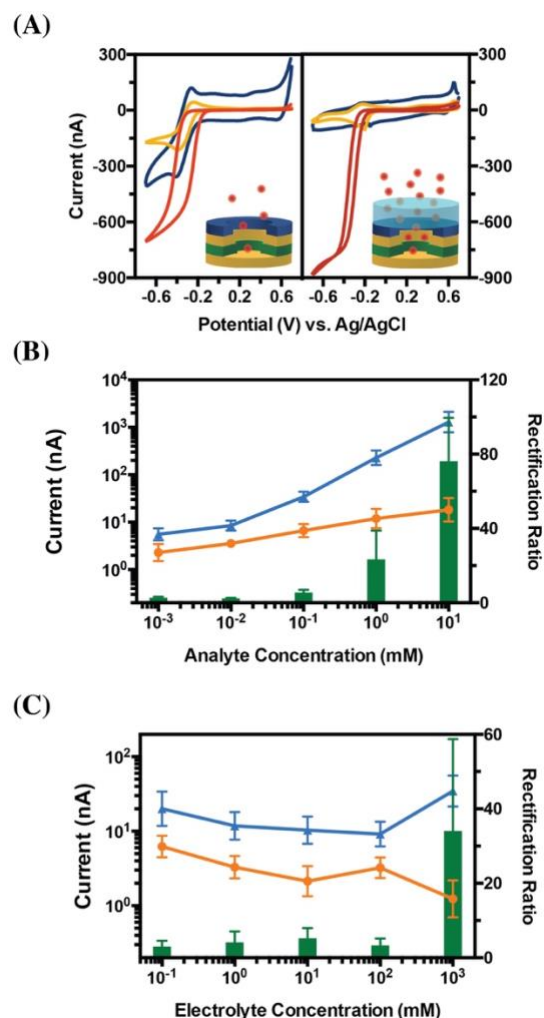


Figure 5. Behavior of Nafion@NEAs in the two-electrode configuration. (A) Comparison of CVs from three different two-electrode configurations implemented either in uncovered NEAs (left panel) or Nafion@NEAs (right panel). In configuration 1 (red), the bottom electrode (BE) and the top electrode (TE) constitute the two terminals, while BE/external Ag/AgCl electrode (orange) are connected as two terminals in configuration 2, and TE/external Ag/AgCl electrode (blue) are connected in configuration 3. (B) Cathodic (blue) and anodic (orange) currents obtained from $\text{Ru}(\text{NH}_3)_6^{3+}$ at varying concentrations in 1 M KCl in Nafion@NEAs, at - 0.5 V and + 0.5 V vs. Ag/AgCl, and corresponding rectification ratios (green bars). Error bars represent the standard deviation over 7 independent devices. (C) Cathodic (blue) and anodic (orange)

currents obtained from $\text{Ru}(\text{NH}_3)_6^{3+}$ in varying background electrolyte concentrations in Nafion@NEAs, at - 0.5 V and + 0.5 V vs. Ag/AgCl, and corresponding rectification ratios. Error bars represent the standard deviation of 4 devices.

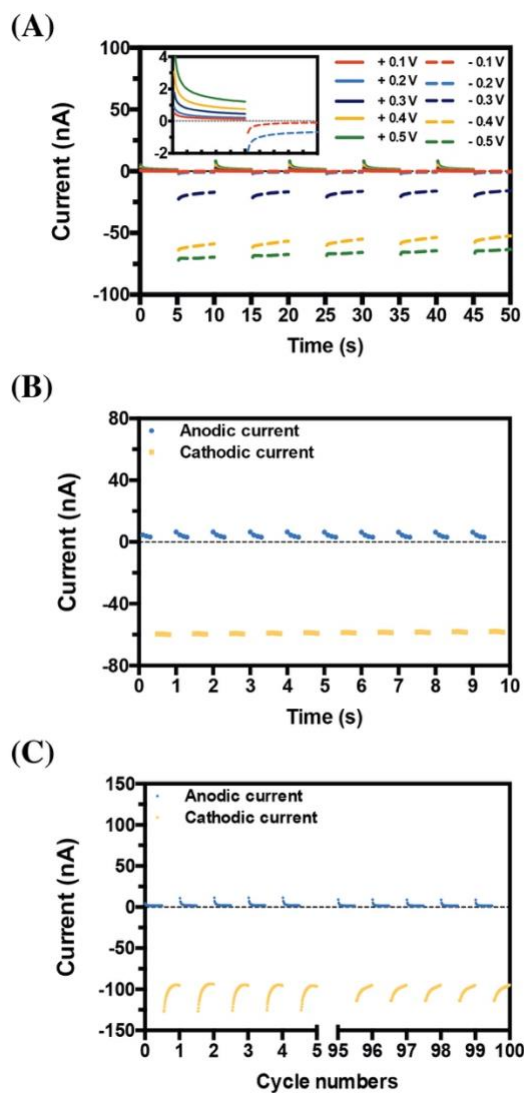


Figure 6. Diode operation of Nafion@NEA. (A) Chronoamperometric plots for 1 mM $\text{Ru}(\text{NH}_3)_6^{3+}$ in 1 M KCl from a Nafion@NEA when switching the potential between oxidizing (from + 0.1 V to + 0.5 V) and reducing (from - 0.1 V to - 0.5 V) potentials for 5 cycles. (*Inset*, Expanded current scale for 1 cycle). (B) Response of Nafion@NEAs, when switching the potential between + 0.5 V and - 0.5 V at 1 Hz. (C) Stability of a Nafion@NEA over 100 cycles. The initial 5 cycles and the last 5 cycles are shown for comparison.

TOC graphic

